J. Fluid Mech. (1992), *vol.* 237, *pp.* 33–56
Printed in Great Britain

Rigid particles suspended in time-dependent flows: irregular versus regular motion, disorder versus order

By ANDREW J. SZERI,[1] W. J. MILLIKEN[2]† AND L. GARY LEAL[2]

[1] Department of Mechanical and Aerospace Engineering, University of California, Irvine, CA 92717, USA

[2] Department of Chemical and Nuclear Engineering, University of California, Santa Barbara, CA 93106, USA

(Received 17 December 1990 and in revised form 3 September 1991)

An experimental and analytical investigation is conducted into the dynamics of small, non-spherical, rigid particles suspended in a flow that is time-dependent from the point of view of the particle, which may be moving. The particles are unaffected by Brownian forces. Of special interest in this study are flows that are *time-periodic* in the Lagrangian frame; this allows for the use of mathematical tools that have been developed for periodically forced differential equations, and for precise and well-characterized experiments. For some classes of periodic flows, it is shown that there exists a global periodic attractor for the orientation dynamics of particles that follow a given particle path, i.e. there is 1 : 1 phase locking of the orientation dynamics with the forcing. This is an important situation because it leads to a strong ordering of an ensemble of particles that follow the same particle path as the flow; such order has significant ramifications for stress and birefringence. In other classes of periodic flows, no such attractor exists; therefore, an ensemble of random initial orientations of the particles on a particle path will not converge and disorder is maintained. Experiments are performed using a computer-controlled four-roll mill to create well-characterized flows in which these various types of dynamical behaviour are realized.

1. Introduction

In this paper, we consider the dynamics of small, non-spherical, rigid particles suspended in flow fields that are unsteady from the point of view of the particle. Our objective is to pursue some of the dynamical possibilities suggested in a recent theoretical analysis of a model microdynamical system by Szeri, Wiggins & Leal (1991), which we refer to hereinafter as SWL. This model system describes the dynamical behaviour of a stretchable, orientable particle suspended in a flowing fluid. The particles in the theory and in the experiments we report here are assumed to be small with respect to lengthscales of the surrounding flow; thus the Reynolds number based on the lengthscale of the particle is small. Note that this does not require the Reynolds number based on the lengthscale of the surrounding *flow* to be small.

Our primary goal is to understand better the behaviour of dilute suspensions of particles. By definition, these suspensions are dilute because the particles are non-

† Present address: Chevron Oil Field Research, 1300 Beach Blvd., La Habra, CA 90631, USA.

interacting; therefore the dynamical behaviour of each particle is not coupled to that of the others. For this reason, it is profitable to study the dynamics of individual particles.

The general problem we address has received much attention in the special case when the flow field is steady in the Lagrangian frame that follows the particle. Jeffrey (1922) derived the evolution equations for the orientation of an ellipsoidal particle in a steady, uniform shear flow. The associated dynamical behaviour was found to be one of two possible varieties: particles of finite aspect ratio rotate periodically following 'Jeffrey orbits', whereas particles of infinite aspect ratio align with the flow direction. Bretherton (1962) extended the analysis of Jeffrey to include the orientation dynamics of particles of more general shapes in a steady, uniform shear flow. Bretherton found that the details of the shape of the particle were not as important as its symmetries. For example, any axisymmetric particle is found to have the same dynamical behaviour in a steady, uniform shear flow as an equivalent ellipsoidal particle.

The dynamical behaviour of particles is much richer in unsteady flows, or more specifically in flows that are unsteady in the Lagrangian frame. The reason is that the orientation dynamics of the particle are forced by the surrounding fluid flow, and the forcing changes over time.

The primary questions that interest us are the conditions for the existence of different types of behaviour in flows that are time-periodic from the point of view of the (perhaps moving) particle: in particular the presence or absence of globally attracting periodic orientations. Because a global periodic attractor is defined over the entire path of the particle, it constitutes a global description of the orientation dynamics of all particles that follow the same path. The physical manifestation of a global periodic attractor for the orientation dynamics is that everywhere along the particle path, there is a favoured orientation of particles (order), which changes, generally, along the particle path. Such a global periodic attractor may be found by consideration of the dynamics of a single particle, although the presence or absence of such an attractor is of greatest importance when one considers an ensemble of particles as in a suspension. In this study, where we consider only one particle at a time, we observe the dynamics of an ensemble of particles that follow a given particle path by repeating experiments with different initial orientations and simply superposing the results.

If the initial state of orientation of the particles in an ensemble is disordered, even isotropic, then a global periodic attractor in the orientation dynamics will cause a convergence of the orientations of the individual particles that follow a given path. In other words, a global periodic attractor for the orientation dynamics leads to order in an ensemble of particles. Note that the word 'global' refers to the product of conformation space and time, and not to physical space. In certain instances, we may find attractors that are global in physical space also, as we shall see. This order yields two important, measurable bulk effects: (i) the (non-Newtonian) stress contribution of the particles will be anisotropic, and (ii) there will be birefringence in systems that exhibit this phenomenon. A more subtle effect of the existence of a global periodic attractor for the orientation is that individual particles forget their initial orientations through a process that does not involve Brownian diffusion. These conclusions are, of course, subject to the assumption of non-interaction of the particles.

Conversely, if there is no such attractor for the orientation dynamics, then a disordered initial state of an ensemble of particles will be maintained along the

particle path through time. Furthermore, individual particles will forever remember their initial conditions, unless there is some Brownian diffusion present.

Attractors for the orientation dynamics are of importance in any type of two-dimensional flow, steady or unsteady. We do not analyse steady flows here because the dynamics of particles in these flows are well characterized; see SWL for a review of the results in two-dimensional flow fields. Dynamical behaviour is not so well characterized in general, unsteady two-dimensional flows. In the present study, we choose to concentrate on time-periodic flows for two reasons. First, time-periodic flows are an important class of flows in technological applications, because they include steady (in a laboratory frame), recirculating flows with spatially inhomogeneous velocity fields. Secondly, these flows are mathematically attractive to study because the periodic nature of the flow allows us to make use of mathematical techniques developed for the treatment of periodically forced ordinary differential equations.

In §2 we give a brief review of the analysis in SWL of the dynamics of particles suspended in two-dimensional flows. We concentrate on the time-periodic case. There is a new discussion about *rotation numbers*, which allow one to classify, exactly, the orientation dynamics of a particle in a given time-periodic flow. We construct arguments to establish the various types of dynamical behaviour in general periodic flows.

In §3, we specialize our analysis to the dynamics of rigid particles in the test section of a four-roll mill. We consider examples of periodic flows that may be realized in the four-roll mill. These flows force some interesting particle dynamics. For some periodic flows, we are able to identify periodic attractors and we observe 1:1 phase locking, whereas for other 'nearby' flows, the test particle tumbles irregularly.

Section 4 is the experimental part of the paper, in which we describe our efforts to observe the predictions of the theory for the example flows analysed in §3. Measurements of the orientation of the particle are taken from photographs of the particle made during its dynamical evolution. In §5, we give our conclusions.

2. The dynamics of particles in unsteady flows

In this section we review the analysis of SWL, as it applies to rigid particles suspended in a flow. In what follows, we assume that the particle in question follows the same path as a fluid element. There is an important distinction to be made between flows that are unsteady from the point of view of the (moving) particle, and those that are steady from this point of view; we refer to such flows as *complex* and *simple* flows, respectively. Complex flows are unsteady in a Lagrangian frame of reference; simple flows are steady. Of course, simple flows are a special case of complex flows.

2.1. *The orientation evolution equations*

Jeffrey (1922) and Bretherton (1962) have demonstrated that the evolution of the orientation of an axisymmetric rigid particle may be described by the vector equation

$$\frac{\mathrm{d}}{\mathrm{d}t}\boldsymbol{R} = \boldsymbol{\kappa}\cdot\boldsymbol{R} - \boldsymbol{\kappa}:\boldsymbol{RRR}, \quad \boldsymbol{\kappa} = \boldsymbol{\Omega} + G\boldsymbol{E}. \tag{2.1}$$

The particle is assumed to be small with respect to lengthscales of the surrounding flow, and unaffected by Brownian forces. The axial (state) vector $\boldsymbol{R}$ gives the instantaneous orientation of the particle. $\boldsymbol{\Omega}$ and $\boldsymbol{E}$ are the vorticity and rate-of-strain

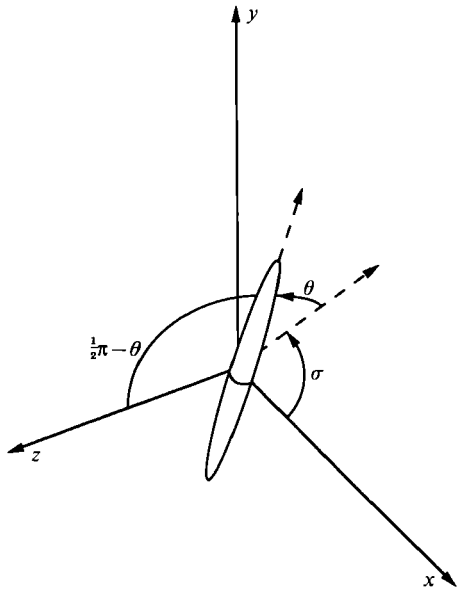

FIGURE 1. Definition sketch of the configuration-space coordinates σ and θ.

tensors, respectively, and the parameter G is the shape factor, which relates the dynamical response of the particle in question to that of an equivalent ellipsoid. The shape parameter normally varies between $G = 0$, which corresponds to a spherical particle, and $G = 1$, which corresponds to a particle with infinite aspect ratio. Physically, the shape factor accounts for the fact that particles of finite aspect ratio rotate less quickly in straining flows than a line element of the fluid. In other words, the competition between the vorticity tensor, which tends to rotate the particle, and the rate of strain tensor, which tends to align the particle along the principal strain axis, is modulated by the shape factor G.

We restrict our analysis to the consideration of particles suspended in two-dimensional flows. We define the Cartesian coordinate system (x, y, z), where the flow occurs in the (x, y)-plane. Note, however, that the axial vector of the particle is free to move out of the plane. In these coordinates, the vorticity and rate-of-strain tensors may be written as

$$\boldsymbol{\Omega} = \begin{bmatrix} 0 & -\frac{1}{2}\omega & 0 \\ \frac{1}{2}\omega & 0 & 0 \\ 0 & 0 & 0 \end{bmatrix}, \quad \boldsymbol{E} = \begin{bmatrix} e & \frac{1}{2}\gamma & 0 \\ \frac{1}{2}\gamma & -e & 0 \\ 0 & 0 & 0 \end{bmatrix}. \tag{2.2}$$

These descriptions involve the flow parameters e (elongation), γ (shear) and ω (vorticity), which depend generally on time either because the flow is unsteady, or because of the motion of the particle through a steady, spatially inhomogeneous velocity field.

We make use of a modified spherical polar coordinate system to describe the orientation of the particle. These coordinates are defined in figure 1. The coordinates are specified in such a way that when $\theta = 0$, the axial vector of the particle lies in the plane of the flow. The axial vector of the particle has Cartesian coordinates

$$\boldsymbol{R} = \begin{pmatrix} \cos\theta & \cos\sigma \\ \cos\theta & \sin\sigma \\ \sin\theta & \end{pmatrix}. \tag{2.3}$$

If one substitutes (2.2) and (2.3) into (2.1), one may obtain separate evolution equations for the angular coordinates. These evolution equations are

$$\dot{\sigma} = \tfrac{1}{2}\omega - Ge \sin 2\sigma + \tfrac{1}{2}G\gamma \cos 2\sigma, \tag{2.4a}$$

$$\dot{\theta} = -\tfrac{1}{2}G(e \cos 2\sigma + \tfrac{1}{2}\gamma \sin 2\sigma) \sin 2\theta. \tag{2.4b}$$

The system (2.4) is a non-autonomous system of ordinary differential equations when the velocity gradient tensor is unsteady from the point of view of the particle. In general, equations (2.4) do not preserve volume in phase space; therefore we anticipate the importance of attractors for the orientation dynamics.

In the very special case of simple flows, the system (2.4) becomes autonomous and may be integrated by quadrature. In either situation (simple or complex) we can exploit the fact that (2.4*a*) is uncoupled from (2.4*b*). Thus we treat the dynamics of the in-plane orientation variable (σ) first, and then consider what happens out-of-plane (θ).

2.2. *Orientation dynamics in general complex flows*

When the surrounding flow is simple, then there are two generic situations. In addition to the vorticity axis, which is never an attractor in two-dimensional flows, there is either no other equilibrium orientation, or there is a stable/unstable pair of equilibrium orientations in the plane of the flow. The globally attracting orientation, if it exists, may be identified by examining the eigenvalues of the system (2.4) evaluated at the equilibria.

In complex flows, on the other hand, there may be an analogous attracting orientation (or orientations) for the particle. However, because the governing equation is non-autonomous, the attracting orientation will generally be time-dependent rather than steady. Thus, we are led to consider directly the relative approach or separation of two distinct orientation time-traces that are solutions of the system (2.4). Two orientations experience a net convergence over a time interval $[0, T]$ whenever the quantity

$$\mathrm{CE}[\sigma_1(0), \sigma_2(0); T] \equiv \int_0^T [2Ge(t) \cos(\sigma_1(t) + \sigma_2(t)) + G\gamma(t) \sin(\sigma_1(t) + \sigma_2(t))]\, \mathrm{d}t \tag{2.5}$$

is positive. We refer to this quantity as the *contraction exponent*. It depends on the initial orientation of the two time-traces, on the time interval, and implicitly on the velocity gradient tensor seen by the two particles, which follow the same path. The time traces $\sigma_i(t)$ of the two orientations must be determined by integration of (2.4*a*). CE is called the contraction exponent because the difference of two orientations changes over the time interval $[0, T]$ as

$$\tan[\tfrac{1}{2}(\sigma_1(T) - \sigma_2(T))] = \tan[\tfrac{1}{2}(\sigma_1(0) - \sigma_2(0))] \exp(-\mathrm{CE}[\sigma_1(0), \sigma_2(0); T]). \tag{2.6}$$

A natural extension of this concept is to the approach or separation of *nearby* orientations. In this situation, one can linearize (2.6) and obtain

$$\epsilon(T) = \epsilon(0) \exp(-\mathrm{nCE}[\sigma(0); T]), \tag{2.7}$$

where the *nearby contraction exponent*,

$$\frac{\mathrm{nCE}[\sigma(0); T]}{T} \equiv \frac{1}{T}\int_0^T [2Ge(t) \cos 2\sigma(t) + G\gamma(t) \sin 2\sigma(t)]\, \mathrm{d}t, \tag{2.8}$$

distinguishes the approach or separation of integral curves near a curve of interest, $\sigma(t)$. In (2.7), $\epsilon(t)$ is a separation in orientation angle.

If one computes the nearby contraction exponent for the full range of initial orientations $0 \leqslant \sigma(0) < \pi$, one may determine which integral curve(s) will attract the others. This procedure varies according to whether the flow parameters are periodic with period T (the special case we concentrate on in the present study), or non-periodic.

The dynamics of the out-of-plane degree of freedom $\theta(t)$ are integrable once the evolution of $\sigma(t)$ is understood. One can derive the solution

$$\tan\theta(T) = \exp\left(-\tfrac{1}{2}\mathrm{nCE}[\sigma(0);T]\right)\tan\theta(0). \tag{2.9}$$

This equation relates the out-of-plane orientation at the end of a time interval to the initial out-of-plane orientation through the dynamics in σ. We note in passing that attracting orientations (with $\mathrm{nCE} > 0$) move toward the plane of the flow.

2.3. *Orientation dynamics in time-periodic flows*

Now we consider the situation that arises when the velocity gradient tensor seen by the particle has a periodic dependence on time. This important situation occurs in many instances, for example: when there are recirculating particle paths through a steady (Eulerian) flow, when a linear (spatially homogeneous) flow varies periodically in time, or when there is a steady Eulerian flow in a spatially periodic domain. The latter situation has been investigated as a model for flow in porous media by Nollert & Olbricht (1985), among others.

The periodic nature of the variation of the velocity gradient tensor with time allows us to make use of some techniques from dynamical systems theory, such as the Poincaré map and rotation numbers of circle maps. The background of these ideas is discussed by Guckenheimer & Holmes (1990), by Wiggins (1988), and by Arnold (1988). The techniques employed below allow one to describe exactly dynamics that are forced in a time-periodic fashion. In our system, the dynamics of interest are the orientation of the particle as a function of time, forced by the time-periodic velocity gradient tensor.

2.3.1. *The Poincaré map*

By knowing how the orientation corresponding to every possible initial orientation evolves over one period of the flow, we know how the orientation evolves for all time, simply by concatenating the solutions for each period. This is the idea behind the Poincaré map, which is defined to be a real-valued function (P) that is exactly equivalent to integrating the differential evolution equations forward for one period of the flow parameters, starting from any arbitrary initial orientation. Thus the Poincaré map evaluated at σ_0 gives the value of σ at the end of the time interval $\sigma_T = \sigma(T;\sigma_0)$, say, for particles that follow a given path. In symbols, $P(\sigma_0) = \sigma(T;\sigma_0)$. A fixed point of k (integer) applications of the Poincaré map corresponds to a periodic integral curve of the corresponding differential equation with a period kT.

An important fact is that (2.4a) is periodic in the angle σ and in time t, when the velocity gradient tensor seen by the particle is periodic with period T. Just as the angles σ and $\sigma + k\pi$ are equivalent, for integer k, we also have equivalence of time t and $t + kT$, as far as the differential equation is concerned. We can think of the integral curves of (2.4a) with periodic flow parameters as lying on the surface of a torus (doughnut), which has coordinates σ around one circular generator and t

around the perpendicular circular generator, as shown in figure 2. The Poincaré map is a map from one t = constant slice of the torus to the (same) slice t = constant + T, which is equivalent to t = constant because t is a cyclic coordinate.

Owing to the nature of the vector field of (2.4*a*) on the torus, integral curves cannot cross one another. In addition the function P is one to one, onto, and differentiable with differentiable inverse (a diffeomorphism).

2.3.2. *Long-time behaviour of arbitrary initial orientations*

As we mentioned, a fixed point of the Poincaré map ($P(\sigma^*) = \sigma^*$) corresponds to a periodic integral curve of the corresponding differential equation. It can be shown that if there is a fixed point of P then all initial conditions are *asymptotically periodic*, i.e. an integral curve that begins at an arbitrary initial orientation will eventually be attracted to the periodic integral curve that corresponds to the (stable) fixed point of the Poincaré map; physically, this is why a particle forgets its initial orientation in a flow where there is a global attractor for the orientation dynamics of particles that follow a given path. If there are no periodic points (for which $P^k(\sigma^*) = \sigma^*$ with $k \geqslant 1$), then there are only complicated, non-periodic (irregular) orbits in the family of solutions to the underlying differential equation. Note that chaotic orbits are precluded in this system owing to the decoupling of the dynamics in σ and θ.

In the case where the fluid flow is steady (in an Eulerian sense) and recirculating, a periodic integral curve of the orientation of period T has a special meaning. It corresponds to a steady orientation in an Eulerian sense. This means that if the orientation of the particles is periodic with the same period as the time it takes for the particles to return to the same spatial location, the orientation of the particles will appear to be constant in a laboratory frame of reference. Moreover, particles on the given path that begin at an arbitrary initial orientation will be drawn to the global attractor. This is why order arises out of a disordered initial ensemble of orientations. Thus finding globally attracting periodic integral curves will be of critical importance in applications, because when they exist, there is a final, ordered state of the system that is steady in an Eulerian sense, and extends over the entire particle path in question.

We remark that neighbouring paths will generally have differing periods, differing velocity gradient tensors, and therefore differing dynamics. Only in flows with spatially homogeneous velocity gradient tensors are the orientation dynamics on one particle path shared by other particle paths.

2.3.3. *Identification of attractors for the orientation dynamics*

Now we move on to see how to find globally attracting periodic integral curves of (2.4*a*). The Poincaré map (of the orientation dynamics of particles that follow a given particle path) is related to the nearby contraction exponent computed over the period of the flow, through

$$\frac{\mathrm{d}P}{\mathrm{d}\sigma_0} = \exp\left(-\mathrm{nCE}[\sigma_0; T]\right).$$

The integral of this equation with respect to σ_0 is

$$P(\sigma_0) = \int_0^{\sigma_0} \exp\left(-\mathrm{nCE}[\lambda; T]\right) \mathrm{d}\lambda + P(0).$$

Here $P(0)$ is the Poincaré map of the origin, a constant. Note that we chose to

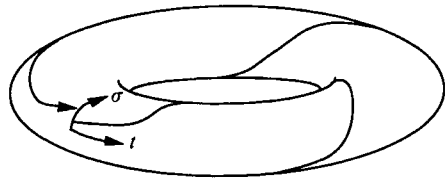

FIGURE 2. A sketch of the space in which solutions of (2.4*a*) lie, when the local flow seen by the particles is periodic in time.

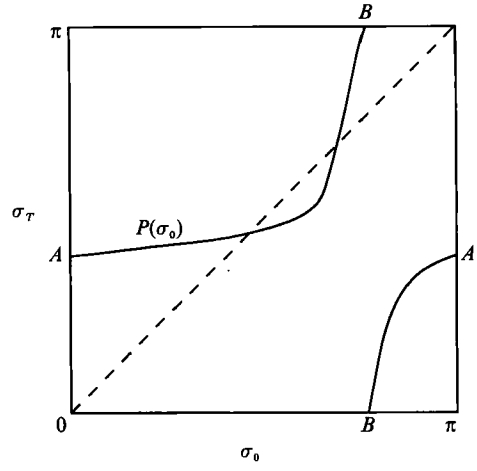

FIGURE 3. Qualitative form of the Poincaré map of (2.4*a*), obtained as the map from a t = constant cross-section of the torus of figure 2 to itself.

perform a definite integration starting from 0; we could have based the integration at a different point, however. One can show that the Poincaré map takes values over the range $P(0) \leqslant P(\sigma_0) < P(0)+\pi$ over its domain $0 \leqslant \sigma_0 < \pi$. This argument is based on the strictly positive derivative of the map, and on the fact that the trajectories cannot cross. This is actually enough information to draw a qualitative picture of the Poincaré map. The Poincaré map must appear like the sketch in figure 3. This picture is drawn in a standard way, in which no distinction is made between equivalent angles such as $\sigma = \alpha+\pi$ where $0 \leqslant \alpha < \pi$, and $\sigma = \alpha$. For this reason, the images of the points 0 and π under the map are equal, and the curve runs off the top of the graph and jumps back onto the bottom.

Fixed points of the Poincaré map are intersections with the line $\sigma_T = \sigma_0$ (where $\sigma_T = \sigma(t = T)$), which is also drawn in figure 3. If there are no intersections of $P(\sigma_0)$ with the curve $\sigma_T = \sigma_0$, then there are no integral curves of period T of (2.4*a*). Note that there may, however, be integral curves of (2.4*a*) of period $kT\,(k > 1)$ corresponding to fixed points of k applications of the Poincaré map.

2.3.4. *Rotation number of the Poincaré map*

The dynamical behaviour of a system that is governed by a map from the circle to the circle, as is our system ($0 \leqslant \sigma < \pi$), may be described compactly by the *rotation number* of the map. The rotation number of a circle map is a single number $0 \leqslant \rho \leqslant 1$ that characterizes the asymptotic behaviour of every possible orbit of the circle map. In our case, where the circle map is a Poincaré map corresponding to a periodically forced differential equation, the rotation number characterizes the

asymptotic behaviour of every possible initial orientation of a particle on a given particle path.

The definition of the rotation number of a circle map is as follows. First, choose an arbitrary point ξ in the interval $[0, \pi)$. Then split up the circle into two sections $I_0 = [\xi, P(\xi))$ and $I_1 = [P(\xi), \xi)$, remembering that values of σ that differ by an integral multiple of π are equivalent. Next, choose another point σ_0. Define $\sigma_k = P^k(\sigma_0)$, i.e. σ_k is the kth iterate of the point σ_0. Then the rotation number is

$$\rho \equiv \lim_{n\to\infty} \frac{1}{n} [\text{cardinality } \{\sigma_k \in I_0, 0 \leqslant k < n\}].$$

(We remind the reader that the cardinality of a set is the number of members.) Thus, *the rotation number is the proportion of iterates of the point σ_0 that fall in the interval I_0*, as the number of iterations tends to infinity. In practice, the rotation number may be computed numerically, with relatively fast convergence.

Now we move on to describe the results about rotation numbers that will be of use to us. The first result we use is that the rotation number is independent of the points ξ and σ_0 used in its definition. Thus, for a single Poincaré map the rotation number needs to be computed only for a single choice of ξ and σ_0. This result may appear quite startling at first glance; it may seem strange that the rotation number calculated from a single initial orientation could characterize the dynamics of every initial orientation. This strong result derives from the properties of the Poincaré map: it is one-to-one, onto, differentiable with differentiable inverse, and preserves the cyclic order of points.

The second important result is that if the rotation number is 0 or 1, then there is a fixed point of the Poincaré map P, i.e. a periodic orbit of (2.4a) of period T. This is easy to see. If there is a fixed point in I_0, then nearly all iterations will fall in I_0 because arbitrary initial conditions are attracted to the fixed point; thus ρ converges to 1. Alternately, if there is a fixed point in I_1, then nearly all iterations will fall in I_1 because arbitrary initial conditions are attracted to the fixed point; this results in ρ converging to 0.

The third result is that if the rotation number is a rational number, say m/n for m, n both integers, then there is a fixed point of P^n, or, equivalently a periodic point of P of period n. Such a point corresponds to a periodic orbit of (2.4a) of period nT. Finally, the fourth result is that if the rotation number is an irrational number, then the Poincaré map has no periodic point of any period. In this case the dynamics of the orientation governed by (2.4a) are strictly non-periodic.

With this information in mind, we proceed to analyse the dynamics of particles in periodic flows as follows. Consider a steady, recirculating flow with a spatially inhomogeneous velocity gradient tensor. The particle paths are nested, closed curves in the plane; these paths are periodic with a period that varies smoothly across particle paths. Along each particle path, particles see a time-periodic local flow. One could consider a 'master' Poincaré map for the orientation dynamics, which would depend on a parameter that serves to label the particle paths in the nested set. For a fixed value of the parameter, we would begin by computing (numerically) the rotation number of the Poincaré map for the in-plane orientation dynamics. If this rotation number is 0 or 1, there must be a fixed point of the Poincaré map, which we may then proceed to find by the intersection of the Poincaré map $P(\sigma_0)$ with the line $\sigma_T = \sigma_0$. Furthermore, we could compute the attractor that passes through σ_0.

If, however, the rotation number converges to a value different from 1, then it is either rational or irrational. Of course, one cannot tell whether the rotation number

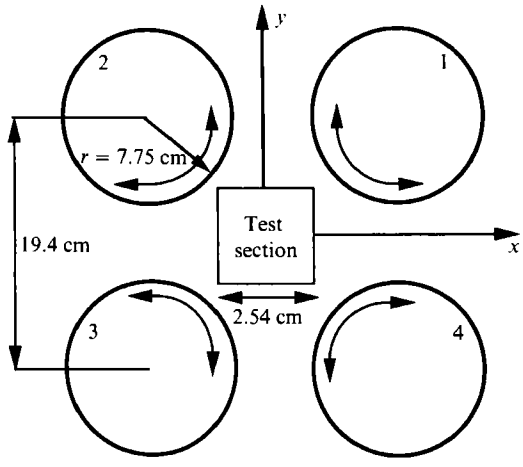

FIGURE 4. Geometry of the four-roll mill used in the experiments.

is rational or irrational, considering the finite precision of the numerical calculation. But suppose that the rotation number varies smoothly over a range of the parameter, i.e. across particle paths. Then we may conclude that it takes infinitely many rational and irrational values. It can be shown in such a situation that the set of parameter values that yield Poincaré maps with irrational rotation numbers has positive measure. Thus if the rotation number varies smoothly over a range of the parameter, we can be certain that some parameter values will lead to irregular motion.

Finally, we remark that there is one special situation where the rotation number gives information that is useful for the whole flow. This is, of course, the case of a spatially homogeneous velocity gradient tensor.

3. Analytical study of particles suspended in the flow in a four-roll mill

In this section, we apply the ideas of the previous section to particles suspended in the flow in a four-roll mill. A four-roll mill is a particularly useful device because one may create nearly two-dimensional flow fields that are well-characterized as linear (spatially homogeneous velocity gradient tensor) in a small test section. A schematic diagram of the particular four-roll mill that we use in the experiments of §4 is shown in figure 4. The flow device consists of a square array of cylinders arranged symmetrically in a square box that is filled with fluid. The test section of the device is the central portion between the cylinders.

Although the discussion in §2 requires that the Reynolds number based on the particle lengthscale be small, it is not necessary that the Reynolds number based on the flow lengthscale be small. However, it is profitable to carry out our physical experiments in a boundary-driven flow at small (flow) Reynolds number. The reason for this is that in such a situation, we have complete and virtually instantaneous control over the details of the flow in the test section by changing the motion of the boundaries; there is no time lag in the control of the flow field owing to inertial effects. In the four-roll mill, if the rollers rotate slowly enough, and if the carrier fluid of the suspension is viscous enough (i.e. if the flow Reynolds number is small), then the flow may be considered inertia-free, to a high degree of accuracy.

3.1. *Governing equations*

In the central test section of the device, the flow is approximately linear and two-dimensional. We define a Cartesian coordinate system in which the flow occurs in the (x, y)-plane, shown in figure 4. As is well known, the velocity gradient tensor may be written in terms of a single flow-type parameter, α, and the strain-rate $\dot{\epsilon}$, in the form

$$\nabla \boldsymbol{u} = \tfrac{1}{2}\dot{\epsilon}\begin{bmatrix} 1+\alpha & -(\alpha-1) & 0 \\ \alpha-1 & -(1+\alpha) & 0 \\ 0 & 0 & 0 \end{bmatrix} + O(x, y). \tag{3.1}$$

The flow-type α ranges between -1 (purely rotational flow) and $+1$ (purely extensional flow); in the case where the rollers change speed, the flow-type α may be a function of time. The stream function corresponding to the flow in the test section is

$$\psi(x, y, t) = \dot{\epsilon}(t)\,(1+\alpha(t))\,xy + \dot{\epsilon}(t)\,(1-\alpha(t))\,(\tfrac{1}{2}x^2 + \tfrac{1}{2}y^2) + O(x^3, x^2 y, xy^2, y^3).$$

One may compute the flow parameters, e, γ and ω, which are required in (2.4):

$$e(t) = \tfrac{1}{2}\dot{\epsilon}(t)\,[1+\alpha(t)], \quad \gamma(t) = 0, \quad \omega(t) = \dot{\epsilon}(t)\,[\alpha(t)-1]. \tag{3.2}$$

Note that the axes we have chosen coincide with the principal axes of the rate-of-strain tensor; this was not necessary for the application of the theory. We remark that the spatial location of the centroid of the particle is unimportant to the dynamics, because the velocity gradient tensor is spatially homogeneous within the test section. Therefore the dynamics of a particle are independent of its spatial location, provided, of course, that the particle remains in the test section of the flow device, where the flow is approximately linear.

The evolution equations for the orientation of the particle corresponding to the system (2.4) are

$$\dot{\sigma} = \tfrac{1}{2}\dot{\epsilon}(t)\,(\alpha(t)-1) - \tfrac{1}{2}G\dot{\epsilon}(t)\,(1+\alpha(t))\sin 2\sigma, \tag{3.3a}$$

$$\dot{\theta} = -\tfrac{1}{4}G\dot{\epsilon}(t)\,(1+\alpha(t))\cos 2\sigma \sin 2\theta. \tag{3.3b}$$

When the particle is an ellipsoid, the shape factor G is known as a function of the aspect ratio. When this is not the case, the dynamics of a general axisymmetric particle are identical to the dynamics of some equivalent ellipsoid. The shape factor of the equivalent ellipsoid must be determined; this is discussed in the Appendix.

3.2. *Dynamics in time-periodic flows*

We consider two examples of the dynamics of rigid particles in time-periodic flows. In the first example, we observe that the dynamics in a time periodic flow are quite different than the dynamics in the time-averaged flow. In the second example, when there is a global periodic attractor, one can observe convergence of distinct initial orientations in a flow that rotates the particles. This latter effect is very different from the dynamics of particles in simple flows, where convergence of distinct initial orientations is observed only in flows that cause steady alignment of particles.

All the mathematical results of this section are computed for a particle with shape factor $G = 0.59$. This shape factor is close to that of the test particle used in the physical experiments of §4. Note, however, that the phenomena we investigate are not peculiar to particles of shape factor $G = 0.59$.

Example 1

Now we consider a one-parameter family of time-periodic flows that force a range of different dynamical responses of the particle. The flow is given by the unsteady flow-type

$$\alpha(\tau) = \eta + 0.1 \sin^2 \pi\tau, \tag{3.4}$$

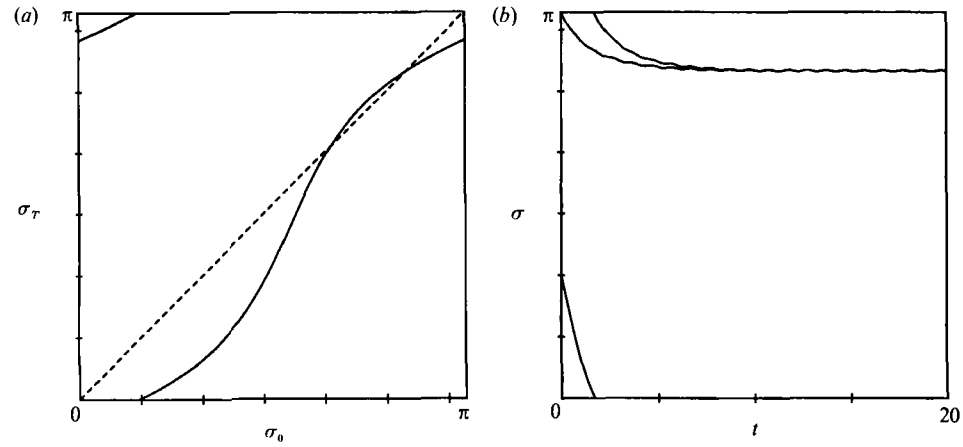

FIGURE 5. (*a*) Poincaré map of the orientation dynamics of particles in the flow in a four-roll mill, with α given by (3.4) with $\eta = 0.3$. (*b*) Solutions $\sigma(t)$ for two different initial orientations, corresponding to (*a*).

which depends on the real parameter η, and is periodic with period 1 in the non-dimensional time $\tau = t\dot{\epsilon}$. We have re-scaled time by the constant, arbitrary strain-rate. Thus the flow parameter α is periodic with forcing period $T_f = \dot{\epsilon}^{-1}$ in the true time variable. In what follows, the periods we report in this example are periods in the true time variable. The period of a periodic response will be denoted T_r.

Physically, increasing η causes an increase in the instantaneous value of α; thus, the flow is characterized by greater rate-of-strain relative to vorticity as η increases. We will show that as the parameter η increases from 0.1 to 0.3, the dynamics of the rigid particle change from irregular behaviour (non-periodic or asymptotically periodic with period $T_r = kT_f, k > 1$) to regular behaviour (asymptotically periodic with period $T_r = T_f$). Also, we will demonstrate that the oscillatory part of the flow radically changes the apparent period of rotation of particles (T_r) compared to the period of rotation in the steady flow where $\alpha = \eta$ or where α is the time-average of (3.4).

The complicated nature of the governing equations (3.3) forced by the time-periodic flow with α given by (3.4) obstructs any attempt at integration in closed form. Therefore we resort to numerical integration by standard methods. We concentrate on the dynamics in the plane of the flow (as described by the dependent variable σ) because the dynamics out of the plane of the flow are integrable once $\sigma(t)$ is known; see (2.9).

If we compute the final orientation after a complete period of the forcing $t = T_f$, beginning at the range of initial conditions $\sigma(0) = 0$ to π, we can assemble a Poincaré map that describes the dynamics in the plane coordinate σ. The map for the case $\eta = 0.3$ is shown in figure 5(*a*). Note the presence of two fixed points, where the Poincaré map crosses the dashed line $\sigma(t = 0) = \sigma(t = T)$. One of these fixed points ($\sigma = 2.6$ radians approximately) corresponds to a globally attracting periodic integral curve and the other ($\sigma = 2.0$ approximately) to a globally repelling periodic integral curve. In figure 5(*b*), we have plotted two example solutions that begin at the initial orientations $\sigma_0 = 0 (= \pi)$ and $\sigma_0 = 1$. Note the quick approach of both orientations to the periodic attractor. Physically, the attractor is characterized by a slight (fine-scale) oscillation about a steady (coarse-scale) alignment. There is no rotation of the particle once its orientation coincides with the attractor in this flow.

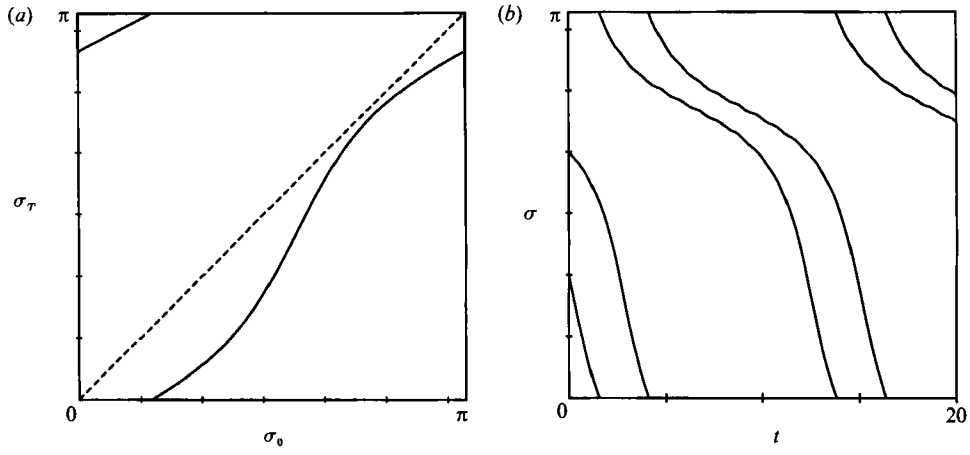

FIGURE 6. Poincaré map of the orientation dynamics of particles in the flow in a four-roll mill, with α given by (3.4) with $\eta = 0.1$. (*b*) Solutions $\sigma(t)$ for two different initial orientations, corresponding to (*a*).

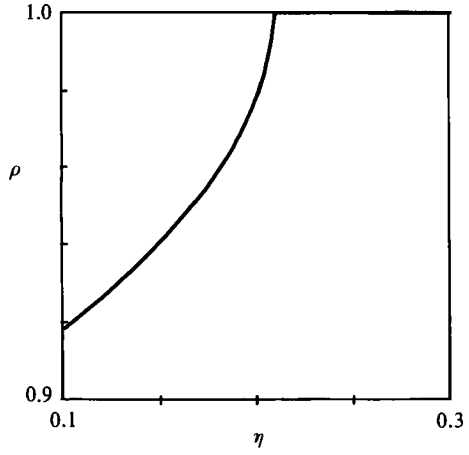

FIGURE 7. Rotation number *vs.* η for the orientation dynamics forced by the flow with α given by (3.4).

In the case $\eta = 0.1$, we obtain the Poincaré map shown in figure 6(*a*). This Poincaré map does not intersect the dashed line $\sigma(t = 0) = \sigma(t = T_f)$; thus there are no fixed points. Two example solutions, with initial conditions $\sigma_0 = 1$ and $\sigma_0 = 2$ are shown in figure 6(*b*). One can observe a slow drifting (coarse-scale) rotation coupled with a fast (fine-scale) oscillation in orientation. If the frequencies of these two motions are precisely commensurate, then the motion is periodic with some period $T_r = kT_f$, $k > 1$. On the other hand, if the ratio of the two frequencies is irrational, then the motion will be non-periodic. In fact, $\eta = 0.1$ is in the parameter range where the rotation number varies continuously, as we now show.

A plot of the rotation number computed over the range of parameter $0.1 \leqslant \eta \leqslant 0.3$ is shown in figure 7. For values of the parameter $\eta_c = 0.21 < \eta \leqslant 0.3$, there is 1:1 phase locking of the orientation dynamics with the forcing, i.e. a global attractor exists and $T_r = T_f$. For values of the parameter $0.1 \leqslant \eta < \eta_c$, the dynamics are either non-periodic or periodic with some period $T_r = kT_f, k > 1$. Thus there is a bifurcation to complicated dynamical response as η decreases through η_c.

As we mentioned, it is easily seen from the time-traces of figure 6(*b*) that the coarse-scale motion of the particles appears to be periodic, with a superposed fine-scale periodic motion. Only when the periods of these two motions are commensurate, is the total motion (coarse- and fine-scale) strictly periodic with some period $T_r = kT_f, k > 1$. In an experiment, the fine-scale motion would be difficult to observe, and so one would only observe the coarse-scale rotation. It is therefore interesting to ask the following question: how does the period of the coarse-scale rotation of a particle subjected to the time-dependent flow (3.4) differ from the period of rotation of the same particle in a 'nearby' steady flow. The period of the coarse-scale rotation for a particle subjected to (3.4) with $\eta = 0.2$ is $T_r = 92T_f$. The period of rotation of a particle subjected to the steady part of the flow (3.4) with $\eta = 0.2$ is $T_r = 17T_f$. Finally, the period of rotation of a particle subjected to $\alpha = 0.25$, the average value of α given by (3.4) with $\eta = 0.2$ over the time interval $[0, T_f = \dot{\epsilon}^{-1}]$, is $T_f = 46T_f$. Thus, if one neglected the time-dependent part of (3.4), the resulting period T_r would be 82% in error. If one simply averaged the time variation of (3.4), the resulting period would be 50% in error. These same effects are observed in the experiments we report in §4.

Example 2

In the second example, we consider the family of periodic flows with strain-rate $\dot{\epsilon}$ and flow-type α given by the following expressions

$$\dot{\epsilon}(t) = 1, \quad \alpha(t) = \begin{cases} -1.0 & nT_f \leqslant t < (n+0.4)T_f, \\ -0.2 & (n+0.4)T_f \leqslant t < (n+1)T_f, \end{cases}$$

where n is a positive integer. It is more convenient to consider the following (equivalent) problem. The strain-rate and flow-type parameter are given by

$$\dot{\epsilon}(t) = T_f, \quad \alpha(t) = \begin{cases} -1.0 & n \leqslant t < (n+0.4), \\ -0.2 & (n+0.4) \leqslant t < (n+1). \end{cases} \tag{3.5}$$

This is a one-parameter family of periodic flows where the parameter is the forcing period itself $T_f = \dot{\epsilon}$. If α were either -1 for all time (fully rotational flow), or -0.2 for all time (predominantly rotational flow), we would observe the particle rotating periodically, with the period of response given by: $T_r = \pi\dot{\epsilon}^{-1}$ and $5.7\dot{\epsilon}^{-1}$, respectively.

It is reasonable that the response of the particle should be different in flows that are identical except for the period of forcing because such flows involve an additional timescale besides the timescale of rotation of the particle in the steady flow $\alpha = -1$ or -0.2. The additional timescale is the period of the forcing. The situation here is somewhat analogous to chaotic particle paths in the blinking vortex (Aref 1984). There, an irregular particle path is produced by subjecting a fluid particle to a periodic repetition of flows, in each of which the motion is regular. The analogy lies in the fact that an irregular motion is produced by adding another timescale to the problem.

This family of flows is particularly interesting because the time average of the flow-type α (which is -0.52) is independent of the forcing period T_f. Thus, different members of this family of flows differ only in the *rate of deformation* $\dot{\epsilon}$, but not in the flow-type, i.e. not in the ratio of rate-of-strain to vorticity. Despite this fact, we shall demonstrate that the dynamics can be markedly different for different periods of the forcing. In particular, we observe that for $0 < T_f \leqslant 3.7$, the particle exhibits irregular rotation, which is either non-periodic or periodic with long period ($T_r = kT_f$, $k > 1$). For forcing periods in the range $3.7 < T_f < 4.9$, however, the motion consists of

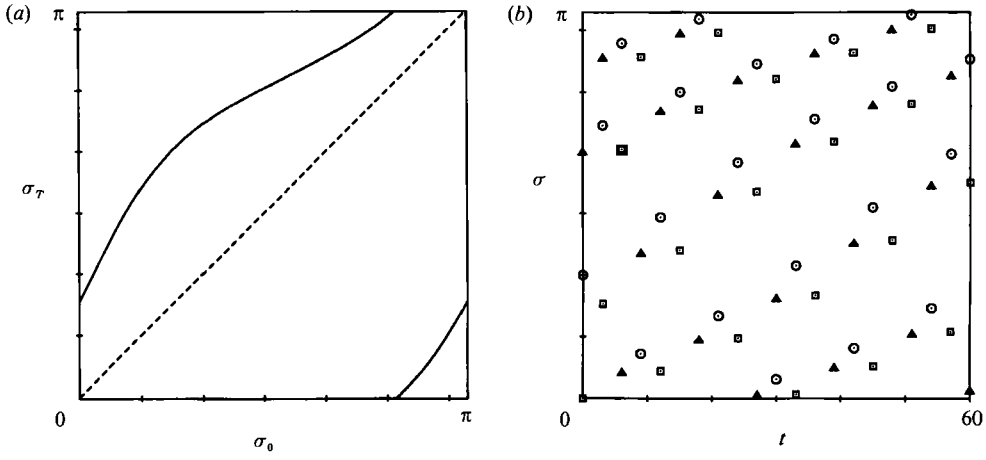

FIGURE 8. (*a*) Poincaré map of the orientation dynamics of particles in the flow in a four-roll mill, with α given by (3.5) with $T_f = 3$. (*b*) Discrete-time snapshots of $\sigma(t)$ for three different initial orientations, corresponding to (*a*).

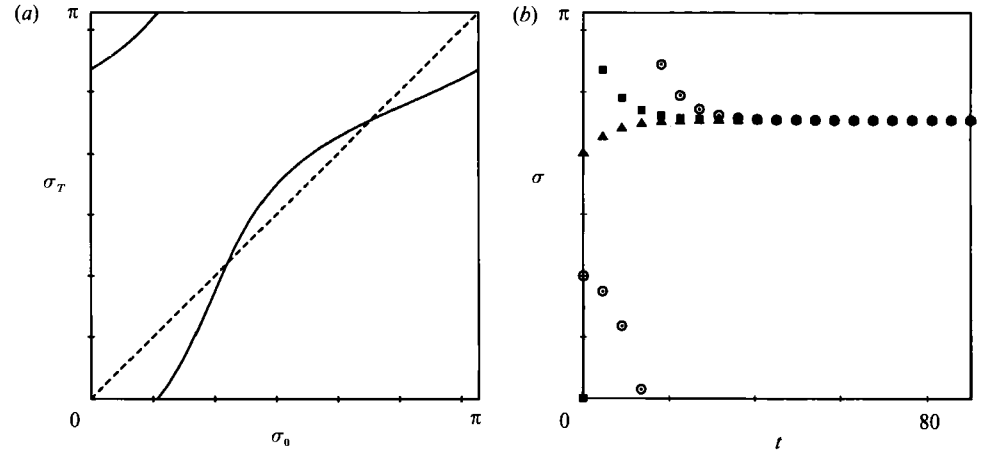

FIGURE 9. (*a*) Poincaré map of the orientation dynamics of particles in the flow in a four-roll mill, with α given by (3.5) with $T_f = 4.5$. (*b*) Discrete-time snapshots of $\sigma(t)$ for three different initial orientations, corresponding to (*a*).

regular rotation after an initial, irregular transient, i.e. all motions are asymptotically periodic with $T_r = T_f$. For forcing periods exceeding $T_f = 4.9$ up to at least 6, the motion is again irregular.

As an example of irregular motion, consider the case $T_f = 3$. The Poincaré map is shown in figure 8(*a*). Note that there is no fixed point. Therefore, we except that this flow is not efficient at promoting order in an ensemble of particles with different initial orientations. Each particle rotates irregularly; thus a picture of the solutions for several initial orientations would be confusing. Instead, in figure 8(*b*) we show snapshots of the orientation angle at periodic intervals of length T_f, for three particles that begin at different orientations $\sigma_0 = 0$, 1 and 2. Note that the scatter of initial orientations is maintained over the time of the experiment ($0 \leqslant t \leqslant 20T_f$). Also, note that each particle remembers its initial condition.

The situation is very different when $T_f = 4.5$. The Poincaré map in figure 9(*a*) shows that there are two fixed points, one stable and one unstable; thus there is 1 : 1

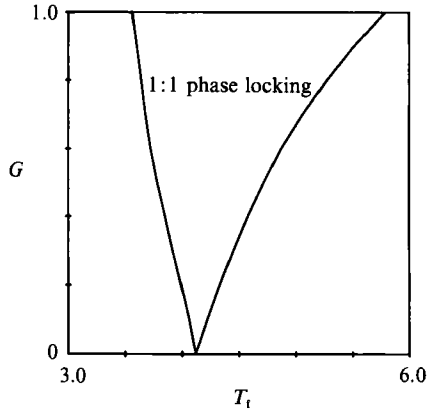

FIGURE 10. A plot of the parameter space of example 2, showing the region in which 1:1 phase locking is manifest.

phase locking of the orientation response with the forcing. The attractor is an orientation that rotates over a period. For simplicity of interpretation we plot the orientation angle at every period of the flow for three different particles in figure 9(*b*). Note the strong tendency of the flow to orient the initially scattered ensemble of orientations. Note also that the particles quickly forget their initial conditions, despite the fact that there are no Brownian forces. This last example shown in figure 9 is yet another illustration of the two most important concepts we want to stress in this study: (i) a global attractor in the orientation dynamics causes an ensemble of initial orientations to become ordered, and (ii) the presence of the attractor results in the forgetting of the initial orientations.

Finally, in figure 10, we show which regions of parameter space (G, T_t) lead to 1:1 phase locking for this example. Note that the range of forcing periods leading to phase locking is most broad when $G = 1$. When $G = 0$, this range narrows to a point. This is due to the fact that the anisotropic terms in (2.4*a*) are multiplied by G. thus when $G = 0$, no anisotropy in particle evolution can develop. We note in passing that other regimes of 1:1 phase locking with $T_t > 6$ were found through numerical experimentation, but we did not pursue these.

4. Experimental study

In this section, we describe the experiments we conducted in a computer-controlled four-roll mill. We begin with a brief description of the apparatus. Next, we report the results of experiments corresponding to examples 1 and 2 of §3.

4.1. *Apparatus*

The experiments were performed on a computer-controlled four-roll mill. This apparatus has been described in detail previously (Bentley & Leal 1986); a brief summary of the key components is included here. The four-roll mill is a device designed to generate a linear, two-dimensional flow. The velocity gradient tensor of this flow, is given by (3.1). Owing to the finite dimensions of the rollers, only a subset of the full range of flows is actually attainable in the laboratory. The apparatus used here produces flow fields that accurately approximate (3.1) for $|\alpha| > 0.2$ in a region about $(2.54\text{ cm})^2$ around the stagnation point (the test section), that lies at the centre of the device. This particular apparatus is distinctive for two reasons: (i) the rollers

are driven by d.c. stepping motors that allow for accurate control of the flow field, and (ii) the particle position within the flow is tracked in real time by a camera and computer.

The apparatus consists of four cylinders (rollers), 17.5 cm in length and 15.5 cm in diameter, positioned in a square array as shown in figure 4. The rollers are situated in a tank 49.5 cm × 49.5 cm and 17.5 cm in depth that is filled with Pale 1000 oil (Caschem, Bayonne, NJ), a polymerized castor oil. The oil is Newtonian with a viscosity of 364 Poise and a density of 1.02 g/cm^3 at 22.5 °C.

The apparatus is equipped with a digital video camera (a charge injection device (CID) Model TN2500, General Electric, Syracuse, NY). The video camera provides input to a Digital Equipment Corporation PDP 11/23 minicomputer, which serves to control the speed of the stepping motors. The computer analyses the video image and determines the centre of mass of the particle in the flow. This information may then be used, if desired, to correct the flow field to account for any disturbance of the particle from the stagnation point of the flow.

When $\alpha > 0$, and the flow is steady, a particle placed near the stagnation point translates away from that point in the direction of the outflow axis, and eventually out of the test section. In order to run experiments for extended lengths of time, the apparatus has been designed with a control scheme that serves to maintain the particle at the stagnation point in steady flows with $\alpha > 0$. The details of the control scheme can be found in Bentley & Leal (1986). The control scheme adjusts the speed of the rollers so as to superimpose a constant (Galilean) correction to the flow field in order to maintain the particle at the stagnation point. This is done in a way that maintains the same flow-type α and strain-rate $\dot{\epsilon}$; the corrections to the flow field are small and imperceptible to the eye. This system can maintain a particle at the stagnation point indefinitely and thus permits experiments to be carried out over long periods of time (hours). One might be concerned that the additional, time-dependent flow due to the control scheme could have an adverse effect on our experiments. However, the orientation dynamics of the particle are forced by the velocity gradient tensor, which is insensitive to the addition of a Galilean flow field.

The particle used in these experiments is a section of optical fibre that is roughly cylindrical in shape. A microscope photograph of the particle is shown in figure 11. The particle has a diameter of 0.089 cm and a length of 0.165 cm which gives it an aspect ratio of 1.85. Our efforts at determining the shape factor of the test particle are described in the Appendix; at present, we simply quote the result $G = 0.56 \pm 0.02$. The density of the rod is slightly greater than that of the fluid; consequently, the rod slowly sinks through the fluid during the experiment. However, owing to the high viscosity of the Pale 1000 oil, this sedimentation amounts to less than 10 cm over the course of a 1 h experiment. Finally, we remark that the Reynolds number based on the diameter of the particle is less than 10^{-5} for the experiments we report below.

4.2. *Examples and discussion*

Now we report the results of physical experiments analogous to examples 1 and 2 of §3.2. The shape factor that we determined by experiment, $G = 0.56 \pm 0.02$, allows us to compare experimental and mathematical results computed for $G = 0.59$.

Example 1

The first example we consider is the family of time-dependent flows described by (3.4). The flow-type α consists of a constant part plus a sinusoidally varying part. We examined the dynamics of the particle orientation as the parameter η in (3.4) was

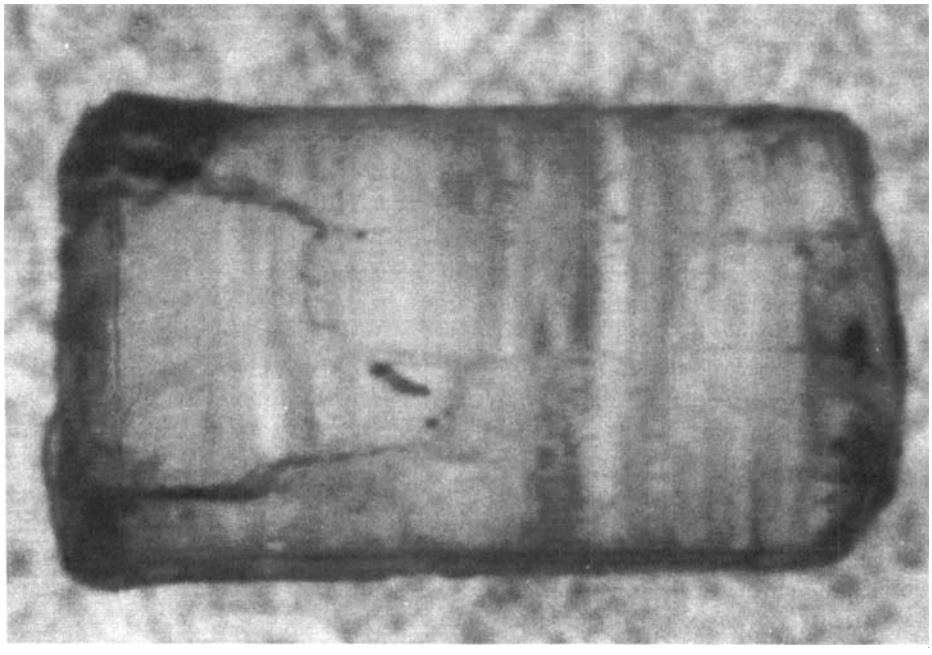

FIGURE 11. Microscopic photograph of the particle used in the experiments. See text for dimensions.

varied. In particular, we wished to determine whether or not the particle rotates in the flow for a given η and if so what is the period of rotation. Note that the control scheme was used during these experiments to maintain the particle at the stagnation point.

We found that for $\eta = 0.27$ and 0.3 the particle in the time-dependent flow (3.4) rotated to a final (attracting) orientation and remained there, as in the mathematical solutions shown in figure 5(*b*). The slight oscillations one notes in the mathematical solution proved to be too small to be observed in the physical experiment. In contrast, continuous rotation of the particle was observed in a steady flow with $\alpha = 0.27$.

For values of $\eta \leqslant 0.25 = \eta_{c,\exp}$, particle rotation was observed, but the period of rotation was dramatically altered by the time-dependent forcing function. In the flow with $\alpha = 0.25 + 0.1\sin^2(\pi\tau)$, the period of rotation was measured as $T_r = 300T_f (= 300\dot{\epsilon}^{-1})$ compared to $20\dot{\epsilon}^{-1}$ for a steady flow with $\alpha = 0.25$. Clearly, the presence of the time-dependent forcing dramatically alters the period of rotation of the particles, in the same way as in the mathematical example in §3.2.

Comparing to the mathematical prediction, we found that particles should experience coarse-scale rotation for values of the parameter $\eta \leqslant 0.21$, which is slightly less than the critical value of 0.25 that we found through experiment. This slight quantitative discrepancy is undoubtedly caused by our uncertainty about the exact value of the shape factor. However, the qualitative agreement between the theory and experiment is excellent.

Example 2

In this example, we consider the orientation dynamics of the particle in the flow described by (3.5). For all values of the forcing period that we investigated ($0 < T_f \leqslant 6$), we found that the particle rotates, as was predicted. Because the

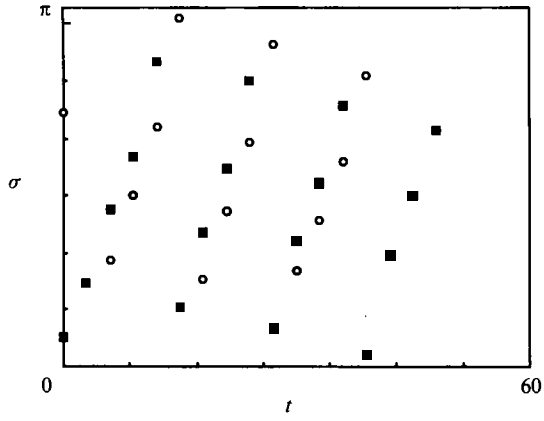

FIGURE 12. Experimental discrete-time snapshots of $\sigma(t)$ for different initial orientations of particles in the flow in a four-roll mill, with α given by (3.5) with $T_f = 3$.

particle is always rotating, it is somewhat difficult to observe an attractor by looking at a full time trace. Therefore, as in §3, we examine snapshots of the orientation at each period of the flow.

The particle was placed at the stagnation point and subjected to the periodic flow described by (3.5). A photograph of the particle was taken at the end of each period of the flow to allow for measurement of the orientation of the particle. This data was then compiled in order to construct an experimental discrete-time map of the orientation dynamics.

One unexpected problem that surfaced during the course of the experiments was that the particle was eventually convected out of the test section of the device for some values of the period. Generally, it was observed that the centre of mass of the particle precessed around the stagnation point. For $T_f = 3.0$ and 6.0 the distance of the particle from the stagnation point increased initially but then decreased. For these periods, the particle did not become removed from the stagnation point by more than about one particle length. In contrast, at $T_f = 4.5$ and 5.0, the particle spiralled away from the stagnation point and out of the test section. This was unexpected, owing to the fact that steady flows with $\alpha < 0$ have generally elliptical (compact) particle paths; in other words points near the stagnation point at the centre of the flow device remain close. Of course the example flow of (3.5) is not steady, but rather periodic in time. It is possible to show that although the stagnation point is stable (in the sense indicated) for the steady flows with $\alpha = -0.2$ and $\alpha = -1.0$, the stagnation point is unstable for the periodic flow when $3.562 \leqslant T_f \leqslant 5.786$. This result is established as follows. When $\alpha = -0.2$ (steady), it is a simple matter to integrate the particle-path equations for any initial location of the particle. This is also true for $\alpha = -1.0$. The particle path in the periodic flow may be found as the set of images of an initial location under a discrete-time map formed by concatenating the solutions over the two sub-intervals of flow given by (3.5). The map is linear without approximation, within the test section of the flow device. Finally, one computes the eigenvalues of this map at the stagnation point to check for stability; when $3.562 \leqslant T_f \leqslant 5.786$, the stagnation point is found to be of saddle type. Thus, if the particle is placed near the stagnation point in the flow (3.5) with $3.562 \leqslant T_f \leqslant 5.876$, it will be carried out of the test section of the flow device. This is but another example of the interesting and non-intuitive dynamics that arise in non-autonomous systems.

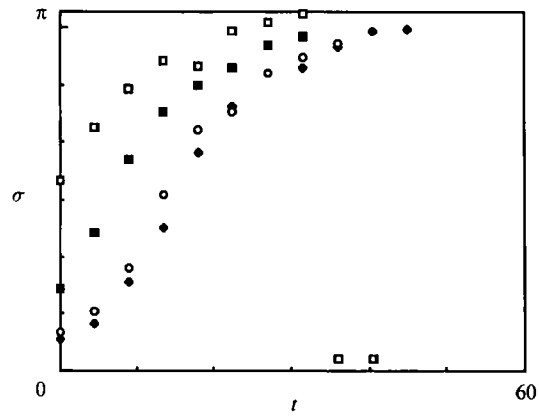

FIGURE 13. Experimental discrete-time snapshots of $\sigma(t)$ for different initial orientations of particles in the flow in a four-roll mill, with α given by (3.5) with $T_f = 4.5$.

The control scheme was designed to operate in flows with $\alpha > 0$, as this is where the need for a control scheme was anticipated. Thus it is not available to us to prevent the particle from being convected out of the test section in the flow of example 2. This unfortunate fact restricts the length of time over which we can conduct experiments for periods in the range $3.562 \leqslant T_f \leqslant 5.786$.

In figure 12, we show the experimentally determined discrete-time map for the orientation dynamics when $T_f = 3.0$. This picture corresponds to the numerically generated map shown in figure 8(*b*). The two figures are remarkably similar and clearly show that there is no attracting (period T_f) orientation. That is to say, at the end of each period of the flow the orientation of each particle is different from that of the previous period. There is also no evidence to suggest that there is an attractor of period other than one, although in practice it is impossible to tell whether these are images of a non-periodic solution or one with a large period, as we have indicated.

The experimentally determined discrete-time map for the orientation dynamics when $T_f = 4.5$ is shown in figure 13. The dynamics here are vastly different from those of figure 12. In figure 13, a pattern of convergence of the ensemble of initial orientations is easily discernable, as in the corresponding, mathematical experiment shown in figure 9(*b*). However, because the particle is quickly convected out of the test section of the flow device, it is not possible to follow the dynamics until full convergence onto the attractor is perceived. Periodic attractors were observed experimentally in this way for forcing periods of 4.0 and 4.5 but not for periods of 3.0, 3.5, 5.0, or 6.0. This is in accord with our theoretical predictions.

Finally, we would like to comment on an interesting connection between orientation dynamics and particle paths in this experiment. Recall that the Poincaré map of the particle paths has a saddle point at the origin when the forcing period is $3.562 \leqslant T_f \leqslant 5.786$. This parameter range corresponds exactly to the parameter range in which the orientation dynamics show evidence of 1:1 phase locking for particles with shape factor $G = 1$ (see figure 10). Particles with this particular shape factor respond dynamically just as a line element of the fluid; thus it is natural that particle paths and orientation dynamics should be strongly related when $G = 1$.

When G is different from 1, the strong connection between particle paths and orientation dynamics is lost. The reason is that whereas particle paths evolve according to the velocity field, the difference between neighbouring particle paths evolves according to the gradient of velocity. Orientation dynamics evolves according

to the tensor $\boldsymbol{\kappa}$, defined in (2.1). When the shape factor $G = \mathbf{1}$, $\boldsymbol{\kappa}$ and the velocity gradient tensor are one and the same; thus the relative motion of nearby particles is related to the orientation dynamics of particles. When the shape factor $G \neq 1$, these two tensors ($\boldsymbol{\kappa}$ and the velocity gradient tensor), and therefore the associated dynamics, are different.

5. Conclusions

In this study, we considered the orientation dynamics of a rigid particle in a flow field, with a view toward better understanding suspensions of such particles. The behaviour of individual particles in steady, spatially homogeneous flow fields has been well understood for some time; therefore we concentrated our efforts on the behaviour of particles in flows that are unsteady from the point of view of the particle. Restricting our inquiry to time-periodic flow fields allowed for the use of the mathematical machinery of Poincaré maps and rotation numbers in our study. Moreover, time-periodic flows proved to be convenient to reproduce in the laboratory in the four-roll mill.

We found that the dynamics of rigid particles in time-periodic flows may be best understood on the basis of whether or not there is a global attractor for the orientation dynamics, where global refers to the product of conformation space and time. When there is such an attractor, a particle that begins at a random initial orientation experiences a transient (non-periodic) response at first, and then settles onto the global periodic attractor. This was demonstrated through mathematical and experimental examples. Furthermore, an ensemble of particles that follow the same (or equivalent) particle path(s) will undergo a strong ordering with regard to orientation, with important ramifications for the state of stress. A last significant point is that particles quickly forget their past configurations; thus memory is a dynamics-dependent as well as material-dependent phenomenon.

Finally, we wish to emphasize that the attractors we have described, and therefore the associated order in the microstructure are phenomena that are global on the particle path in question. At any point in space and time along a particle path where there is a global attractor for the orientation dynamics, there is (i) a single attracting orientation and (ii) a locally ordered state of the particles given by the attractor.

This work was supported, in part, by grants from the Office of Naval Research, and by the Fluid Mechanics Program of the National Science Foundation.

Appendix. Determination of the particle shape factor

In this Appendix, we describe our efforts to determine an appropriate shape factor G of the test particle. Using the four-roll mill, we have arrived at two methods for the experimental determination of the shape factor. We describe these techniques first. Thereafter, we give the results of the experiments, and compare with analytical methods of establishing the shape factor.

Method 1. *Orientation of the particle in a steady flow*

In the special case of a steady flow in a four-roll mill, there is a single attracting orientation whenever the discriminant

$$D = G^2(1+\alpha)^2\dot{\epsilon}^2 - (1-\alpha)^2\dot{\epsilon}^2$$

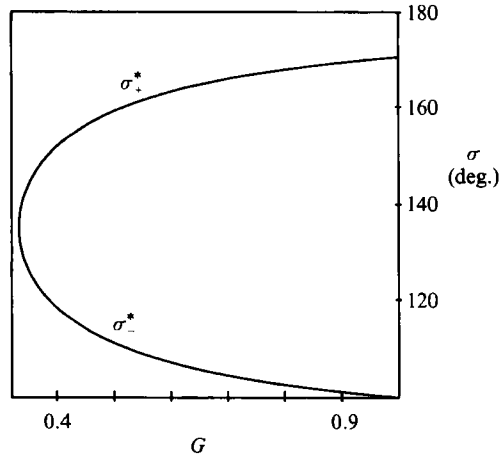

FIGURE 14. Equilibrium orientation (σ) in degrees *vs.* shape factor (G) for steady flow in a four-roll mill, $\alpha = 0.5$. The upper branch, labelled σ_+^*, is the branch of globally attracting equilibria.

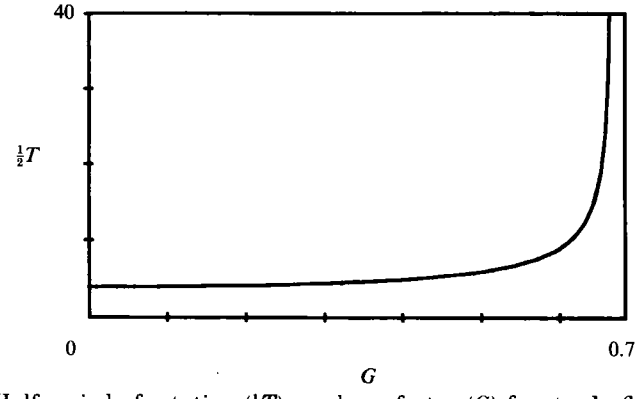

FIGURE 15. Half-period of rotation ($\frac{1}{2}T$) *vs.* shape factor (G) for steady flow in a four-roll mill, with $\alpha = 0.2$ and $\dot{\epsilon} = 1$.

is positive. The stable, globally attracting orientation in this case is $(\sigma, \theta) = (\sigma_+^*, 0)$, where

$$\tan \sigma_\pm^* = \frac{-G(1+\alpha)}{1-\alpha} \pm \frac{(G^2(1+\alpha)^2-(1-\alpha)^2)^{\frac{1}{2}}}{1-\alpha}.$$

Thus, for a given value of α, we can use the final, stable orientation of a particle in the flow to determine the shape factor. An example of this is given in figure 14, where we show the curve of equilibrium orientations versus shape factor G for a steady flow with $\alpha = 0.5$. One need only observe the final orientation of the particle in an experimentally produced flow, and then read off the effective shape factor G.

Method 2. Rotation of the particle in a steady flow

Alternately, one can obtain the shape factor from the period of rotation of the particle in a steady flow with $D < 0$. The formula for the half-period of rotation $\frac{1}{2}T$ is

$$\tfrac{1}{2}T = \frac{\pi}{(-D)^{\frac{1}{2}}}.$$

In figure 15, we have plotted the half-period $\frac{1}{2}T$ as a function of shape factor G for flow-type $\alpha = 0.2$ and $\dot{\epsilon} = 1$. To determine G, one simply measures the period of

α	Final orientation[a]	Period of rotation[b]	G
0.3	2.56		0.58
0.4	2.72		0.58
0.5	2.85		0.58
0.5	2.85		0.58
0.7	3.03		0.80
0.8	3.07		0.70
0.2		11.3	0.48
0.2		13.2	0.54
0.2		13.1	0.54
0.22		14.6	0.53
0.27		20.3	0.53

[a] In radians; obtained by method 1.
[b] In dimensionless time units; obtained by method 2.

TABLE 1. Experimental determination of the shape factor G

rotation at a given α, and reads off the value of G from the curve. Clearly, this technique is accurate only for the range of G where there are significant changes of G with α. In figure 15, where $\alpha = 0.2$, this range corresponds to $0.5 \leqslant G \leqslant 0.7$. For other values of α, the range of accurate determination of G shifts.

Experimental determination of the shape factor

The shape factor G may also be determined by analytical means. The aspect ratio of the particle used in our experiments was 1.85; for *ellipsoids* of this aspect ratio, the shape factor would be $G = 0.54$. Using slender body theory, Cox (1971) has derived an expression for the equivalent (ellipsoidal) aspect ratio for particles with blunt ends. Because the aspect ratio of this rod is moderate, however, one can only hope to obtain a rough estimate of the shape factor using this technique. The equivalent aspect ratio for this particle is found by Cox's method to be 2.92, which corresponds to a value $G = 0.79$. The broad range of shape factors obtained by analytical methods (0.54 to 0.79) indicates that an experimental determination is required.

In experiments, it was observed that the rod exhibited a periodic rotation in the flow field for steady flows with $\alpha \leqslant 0.27$. The period of this rotation was measured and found to be approximately constant over 10 periods. However, the rate of rotation of the rod was not steady but rather varied in systematic fashion reminiscent of 'Jeffrey orbits'. For $\alpha \geqslant 0.3$, the rod rotated monotonically to a particular, steady orientation that depends on α. Based upon these results, the sign of the discriminant D must change between $\alpha = 0.27$ and $\alpha = 0.3$. This bounds the shape factor to the range $0.54 < G < 0.58$.

The shape factor G can be obtained from steady experiments using methods 1 and 2, outlined above; see table 1 for the results of these experiments. The two methods gave very similar results, except for trials of method 1 with $\alpha = 0.7$ and 0.8. The dissimilar results for $\alpha = 0.7$ and 0.8 reflect the difficulty we had in accurately measuring the small angles of the final orientations of the particle. Moreover, small departures from axisymmetry or fore–after symmetry of the particle could have been reflected in the slight spread of the data. In summary, the best value of G we determined to be 0.56 ± 0.02, which is quite close to that of an ellipsoidal particle of the same aspect ratio.

REFERENCES

AREF, H. 1984 Stirring by chaotic advection. *J. Fluid Mech.* **143**, 1–21.

ARNOLD, V. I. 1988 *Geometrical Methods in the Theory of Ordinary Differential Equations*. Springer.

BENTLEY, B. J. & LEAL, L. G. 1986 A computer-controlled four-roll mill for investigations of particle and drop dynamics in two-dimensional linear shear flows. *J. Fluid Mech.* **167**, 219–240.

BRETHERTON, F. P. 1962 The motion of rigid particles in a shear flow at low Reynolds number. *J. Fluid Mech.* **14**, 284–304.

COX, R. G. 1971 The motion of long slender bodies in a viscous fluid. Part 2. Shear flow. *J. Fluid Mech.* **45**, 625–657.

GUCKENHEIMER, J. & HOLMES, P. 1990 *Nonlinear Oscillations, Dynamical Systems, and Bifurcations of Vector Fields*. Springer.

JEFFREY, G. G. 1922 The motion of ellipsoidal particles immersed in a fluid. *Proc. R. Soc. Lond.* A **102**, 161–179.

NOLLERT, M. U. & OLBRICHT, W. L. 1985 Macromolecular deformation in periodic extensional flows. *Rheo. Acta* **24**, 3–14.

SZERI, A. J., WIGGINS, S. & LEAL, L. G. 1991 On the dynamics of suspended microstructure in unsteady, spatially inhomogeneous, two-dimensional fluid flows. *J. Fluid Mech.* **228**, 207–241.

WIGGINS, S. 1988 *Global Bifurcations and Chaos–Analytical Methods*. Springer.